

Optimization of friction stir welding process parameters to maximize tensile strength of stir cast AA6061-T6/ AlN_p composite



B. Ashok Kumar^{a,*}, N. Murugan^{b,1}

^a Department of Mechanical Engineering, Faculty of Engineering, Erode Builder Educational Trust's Group of Institutions, Nathakadaiyur, Kangayam 638 108, Tirupur District, Tamil Nadu, India

^b Department of Mechanical Engineering, Coimbatore Institute of Technology, Coimbatore 641 014, Tamil Nadu, India

ARTICLE INFO

Article history:

Received 11 October 2013

Accepted 22 December 2013

Available online 8 January 2014

Keywords:

A. Aluminium metal matrix composite

B. Particulates

D. Welding

ABSTRACT

Aluminium Matrix Composites (AMCs) reinforced with particulate form of reinforcement has replaced monolithic alloys in many engineering industries due to its superior mechanical properties and tailorable thermal and electrical properties. As aluminium nitride (AlN) has high specific strength, high thermal conductivity, high electrical resistivity, low dielectric constant, low coefficient of thermal expansion and good compatibility with aluminium alloy, Al/AlN composite is extensively used in electronic packaging industries. Joining of AMCs is unavoidable in many engineering applications. Friction Stir Welding (FSW) is one of the most suitable welding process to weld the AMCs reinforced with particulate form of ceramics without deteriorating its superior mechanical properties. An attempt has been made to develop regression models to predict the Ultimate Tensile Strength (UTS) and Percent Elongation (PE) of the friction stir welded AA6061 matrix composite reinforced with aluminium nitride particles (AlN_p) by correlating the significant parameters such as tool rotational speed, welding speed, axial force and percentage of AlN_p reinforcement in the AA6061 matrix. Statistical software SYSTAT 12 and statistical tools such as analysis of variance (ANOVA) and student's t test, have been used to validate the developed models. It was observed from the investigation that these factors independently influenced the UTS and PE of the friction stir welded composite joints. The developed regression models were optimized to maximize UTS of friction stir welded AA6061/ AlN_p composite joints.

© 2014 Elsevier Ltd. All rights reserved.

1. Introduction

AMCs reinforced with particulate form of reinforcements find extensive applications in sports equipment, automotive and aerospace industries due to its superior mechanical, thermal and tribological properties as compared with its corresponding monolithic alloys [1,2]. As those properties of AMCs are tailorable by changing the weight percentage of reinforcement in the matrix, their usage has enormously increased. AMCs reinforced with particulate form of ceramics are particularly attractive due to its isotropic properties, higher operating temperature, oxidation resistance, ease of fabrication over the other geometries of reinforcement such as flake and fiber [3]. To enhance the effective use of AMCs, secondary processes such as joining and machining are as equally significant as the fabrication of AMCs. Joining of AMCs by traditional fusion

welding processes which are normally applied to Al alloys results in reduced joint strength due to oxide inclusions, solidification shrinkage, porosity, distortion, more residual stress, formation of intermetallic compounds due to chemical reactions between matrix and reinforcement, etc. [4]. Al alloy matrix heated to its melting point is the primary reason for the above said problems. If AMCs are welded by solid state welding process, these problems can be eliminated [4].

Friction stir welding is a low heat input solid state welding process invented by The Welding Institute, UK in 1991 [5]. A non-consumable rotating hard tool is used to plasticize the abutting surfaces of the plates to be joined by generating a frictional heat and to stir the plasticized material from the advancing side to the retreating side of the tool and consolidate at the retreating side by the axial force acting through the tool shoulder. A detailed description about the FSW process is presented in literature [6,7]. FSW was initially intended to weld aluminium based low melting point alloys. Due to the success of FSW process to weld Al alloys, FSW was used for other monolithic alloys such as magnesium and copper [8,9] and then extended to weld high melting point materials such as nickel, mildsteel and stainless steel [7,10–12]. For the past one decade, FSW has been successfully employed to

* Corresponding author. Tel.: +91 4257 241935, mobile: +91 9942699429; fax: +91 4257 242007.

E-mail addresses: ashokbkumar@yahoo.com (B. Ashok Kumar), murugan@cit.edu.in (N. Murugan).

¹ Tel.: +91 422 2574071/2574072, mobile: +91 9751824123; fax: +91 422 2575020.

weld advanced materials like AMCs reinforced with hard ceramics materials such as SiC, Al_2O_3 , B_4C , TiB_2 , TiC and ZrB_2 [13–18].

In the welding of AMCs, FSW process produces remarkable weld quality as compared to the weld produced by fusion welding process. In FSW process, reinforcement particles are not agglomerated in the weld zone as it gets agglomerated in the case of fusion welding process. Also reinforcement particles are distributed uniformly in the weld zone even though reinforcement particles are agglomerated in base material [19]. In addition to that, due to the dynamic recrystallization and reduction of Al matrix grain size in the weld zone by the intense stirring of material, mechanical properties of friction stir welded joints are comparable with those of base composite [14]. Joint efficiency of friction stir welded AMCs was reported above 95% under the optimized FSW process condition [17,18]. As FSW process produces superior weld quality under optimized process condition, currently it is successfully employed in many engineering fields such as aerospace, shipbuilding and military applications where high quality weld is required [20].

Among the various FSW process parameters such as tool rotational speed, welding speed, axial force, tool geometry, tool material, tool tilt angle, clamping force and geometry, the first four parameters play a significant role to produce sound weld joints. Tool rotational speed influences the temperature in the stir zone and subsequent grain growth [21]. Higher tool rotation rates generate higher frictional heat due to higher relative motion between the tool and substrate and result in more intense stirring and mixing of material [22]. The rate of stirring of plasticized material determines the formation of defects in the weld zone. Excessive stirring of plasticized material will result in tunnel defects. Lack of stirring will result in lack of bonding. Azimzadegan and Serajzadeh [23] observed an increase in the width of stir zone with increased tool rotational speed. The welding speed determines the exposure time of this frictional heat per unit length of weld and subsequently affects the grain growth [24]. The rate of heating in a thermal cycle during FSW is a strong function of the welding speed. Increase in welding speed causes a decrease in frictional heat generation and lack of stirring [25]. The welding speed also influences the width of the stir zone. The welding speed prompts the linear motion of tool which in turn moves the plasticized material from the front to the back of the tool pin and completes the welding.

As the axial force increases, both hydrostatic pressure beneath the shoulder and the temperature in the stir zone will increase. The hydrostatic pressure should be higher than the flow stress of the materials to be welded. Axial force is also responsible for flash formation. An excessive axial force results in higher amount of flash leading to defects [26]. The shoulder force is directly responsible for the plunge depth of the tool pin into the substrate [27]. FSW tool geometry is another significant parameter to influence the material flow and weld joint properties. Material flow is predominantly influenced by the FSW tool profiles, FSW tool dimensions and FSW process parameters [25]. The FSW tool is harder than the material to be welded. The tool plays the following three major roles in the formation of the joint [28]: (1) Generate the frictional heat beneath the shoulder. (2) Extrude the plasticized material from the front to the back of the tool pin and, (3) forge the plasticized materials by its shoulder. The formation of various regions of friction stir welded joint is affected by the material flow behavior under the action of rotating non-consumable tool.

Some of the tool pin profiles analyzed by the researchers are straight and draft type of cylindrical, square, triangular, hexagonal, octagonal and cylindrical threaded. Elangovan and Balasubramanian [25] attempted to weld AA2219 aluminium alloy by various profile tool pins such as straight cylindrical, taper cylindrical, threaded cylindrical, straight square and straight triangular. It was found that straight square profile pin gave better tensile

strength among the other tool pins. Vijay and Murugan [29] developed the different FSW tool pin profiles viz., straight square, straight hexagon, straight octagon, taper square, taper hexagon and taper octagon with different shoulder to pin diameter (D/d) ratio of 2.8, 3 and 3.2 to weld the in situ Al-6061-10 wt% TiB_2 composite and studied the effect of tool pin profile on metallurgical and mechanical properties of the weldments. It was found that straight square profile tool pin with the D/d ratio of 2.8 exhibited better joint strength with fine grains at the weld zone when compared to the other pin profiles.

From the literature of FSW of AMCs [17,18] it is evident that joint strength of friction stir welded composite is highly influenced by percentage of reinforcement in the composite. Fogagnolo et al. [30] studied the UTS of Al matrix composites reinforced with 5 wt% AlN and 15 wt% AlN produced by mixing the Al and AlN powder by two process namely (a) conventional mixing and (b) mechanically alloying and then these powder mixtures were consolidated by cold-pressing followed by hot extrusion. Surprisingly, UTS of composite containing 15% AlN was less than that of composite containing 5% AlN produced by both the processes. It was justified that sharp angles and cracks usually present in the particulate reinforcements and agglomeration of reinforcement increased the stress concentration and affected the UTS. In higher reinforcement (15 wt% AlN) composite, possibilities of above defects were more as compared to the composite containing less reinforcement (5 wt% AlN). Hence in this study, percentage of reinforcement was also taken as a parameter to obtain the maximum UTS of the composite. Al/SiC and Al/AlN composites are extensively used as electronic packaging materials [31]. Even though the thermal conductivity of AlN (175 W/m K) is less than SiC (250 W/m K), AlN is chemically more stable than SiC at higher temperatures. Aluminium does not react with AlN [31] whereas in Al/SiC composites, Al reacts with SiC and forms brittle Al_4C_3 phase which deteriorates the mechanical properties of Al/SiC composite [32].

In the present work, an attempt has been made to join the AA6061/AlN_p composite by FSW process. The four factor, five level central composite rotatable design matrix was adopted to carry out the experiments to reduce the number of experimental runs. Two regression models were developed to correlate the significant parameters such as tool rotational speed, welding speed, axial force and percentage of reinforcement with the UTS and PE of friction stir welded AA6061/AlN_p composite. The developed regression models have been optimized by using the generalized reduced gradient method to attain the maximum UTS in three different situations as follows: (i) maximizing the UTS, (ii) maximizing the UTS at higher welding speed and (iii) maximizing the UTS and PE at higher welding speed.

2. Scheme of investigation

2.1. Production of AA6061/AlN_p composite

AA6061/AlN_p composite was produced by stir casting technique. An indigenously developed modified electric stir casting furnace with bottom pouring arrangement was used to fabricate the composite. Cleaned extruded aluminium alloy (AA6061-T6) rods of 25 mm diameter were loaded inside the coated stainless steel crucible and the temperature of the electric furnace was set to 1000 °C. The chemical composition of AA6061 alloy is presented in Table 1. The melt was stirred by a coated stainless steel stirrer coupled with electric motor to facilitate both incorporation and uniform distribution of the AlN_p reinforcement in the molten Al alloy. The crucible and stirrer were coated to avoid any contamination at higher temperature. A predetermined quantity of preheated AlN_p of size 3–4 µm was added into the melt at the side of the vortex. To increase

Table 1

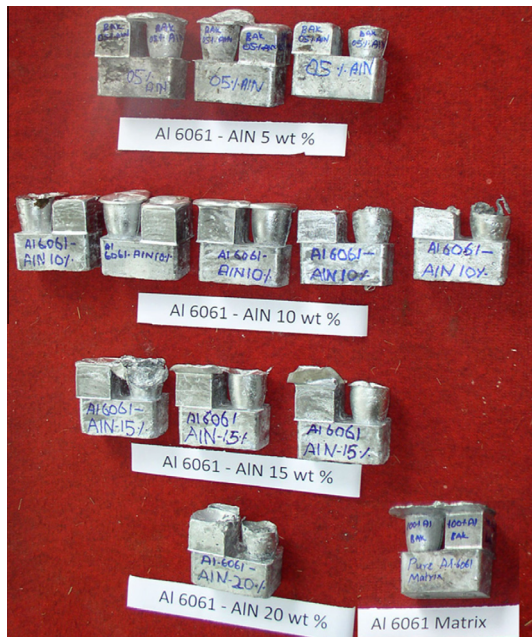
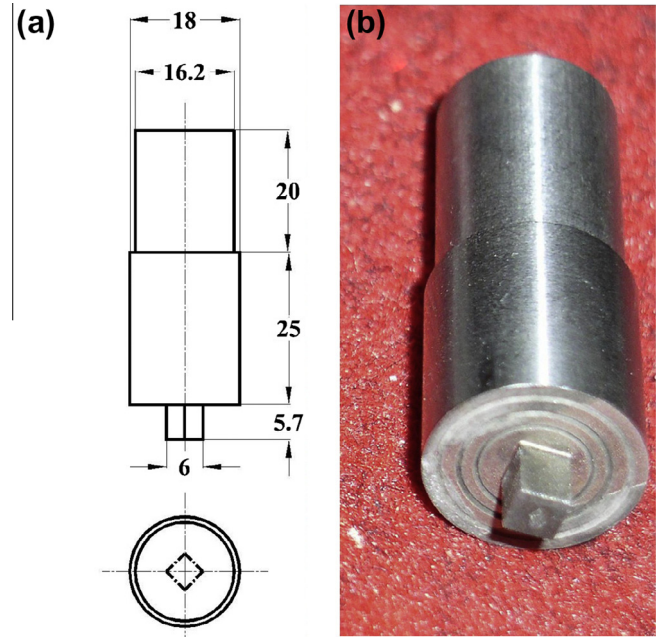
The chemical composition of AA6061-T6 alloy matrix.

Element	Mg	Si	Fe	Mn	Cu	Cr	Zn	Ni	Ti	Al
wt%	0.9	0.64	0.26	0.1	0.21	0.05	0.04	0.02	0.01	Balance

the wettability of AlN_p reinforcement with Al alloy matrix, magnesium of 2 wt% of total weight of the composite to be produced was added into the melt. AlN_p were incorporated into the melt for 260 s. The mixture of molten aluminium and AlN_p were further stirred for 1200 s and then poured into a preheated permanent mould of size 100 mm × 50 mm × 50 mm through bottom pouring arrangement. Argon gas was supplied at a constant flow rate of 2 lpm into the furnace when its temperature reached 650 °C till the molten composite was poured into the permanent mould. Similarly various AA6061/ AlN_p composites containing 0–20 wt% of AlN_p were produced. The detailed description of fabrication of AA6061/ AlN_p composite is given elsewhere [32]. Fig. 1 depicts the AA6061/ AlN_p composites produced from stir casting route. From the composite block, plates of size 100 mm × 50 mm × 6 mm were cut to perform FSW trail runs to fix the range of process parameters and carryout FSW of composites as per design matrix.

2.2. Identification of process parameters

From the literature it was found that, the most significant parameters which influence the mechanical properties of the friction stir welded AMC joints are tool rotational speed, welding speed, axial force, tool pin profile and percentage of reinforcement of the ceramic particles in the composites. As square profile tool pin gave better joint strength, it was decided to fabricate FSW tool pin of square profile without draft from High Carbon High Chromium (HCHCr) steel material. The tool was produced using Computerized Numerically Controlled (CNC) turning centre and Electrical Discharge Machine (EDM) and were oil hardened to obtain a hardness of 60–62 HRC. The geometry and dimensions of the tool are presented in Fig. 2.

**Fig. 1.** The fabricated stir cast AA6061/ AlN_p composites.**Fig. 2.** Square profile tool pin: (a) dimensions of tool and (b) fabricated tool.

2.3. Finding out the limits of identified process parameters

To fix the working range of FSW process parameters chosen for this study such as tool rotational speed, welding speed and downward axial force, many trial experiments were conducted on AA6061/ AlN_p composites. The feasible limits of FSW process parameters were chosen in such a way that the friction stir welded joints shall be free from any macro level defects such as tunnel defect, pin hole and crack. The feasible range of process parameters for obtaining defect free welds of AMCs is narrower than that of the unreinforced monolithic alloys due to less ductility of AMCs resulting from the presence of ceramic particles [33]. Again, as the ductility of cast AMC is lesser, the feasible range of FSW parameters is still narrower [18]. The upper limit of the each parameter is coded as +2 and the lower limit as −2, the coded values for intermediate ranges are calculated using the Eq. (1) [34].

$$X_i = 2[2X - (X_{\max} + X_{\min})]/(X_{\max} - X_{\min}) \quad (1)$$

where X_i is the required coded value of a variable X ; X is any value of the variable between X_{\max} and X_{\min} ; X_{\max} is the upper limit of the variable; X_{\min} is the lower limit of the variable. The chosen levels of the process parameters with their notations and units are presented in Table 2.

2.4. Developing an experimental design matrix

The four factor, five level central composite experimental design matrix selected to conduct the experiments consists of 31 sets of coded conditions is shown in Table 3. The first 16 experimental runs are derived from full factorial experimental design matrix ($2^4 = 16$). The next 8 experimental runs comprise a combination of each process variable at either their lowest (−2) or highest (+2) level with the other three variables at the intermediate level

Table 2
Process parameters and its levels.

S.No.	Parameter	Notation	Unit	Levels				
				–2	–1	0	+1	+2
1	Tool rotational speed	<i>N</i>	rpm	1000	1100	1200	1300	1400
2	Welding speed	<i>S</i>	mm/min	25	40	55	70	85
3	Axial force	<i>F</i>	kN	3	4	5	6	7
4	% of AlN _p	<i>R</i>	wt%	0	5	10	15	20

Table 3
Design matrix and experimental results.

Test run	Design matrix				Joint properties		
	Process parameters				UTS (MPa)	PE (%)	Joint efficiency (%)
	N	S	F	R			
R01	–1	–1	–1	–1	150.01	4.54	82.88
R02	+1	–1	–1	–1	159.13	4.14	87.92
R03	–1	+1	–1	–1	133.20	4.62	73.59
R04	+1	+1	–1	–1	146.21	4.48	80.78
R05	–1	–1	+1	–1	144.65	4.12	79.92
R06	+1	–1	+1	–1	143.68	3.44	79.38
R07	–1	+1	+1	–1	138.64	4.46	76.60
R08	+1	+1	+1	–1	141.86	4.11	78.38
R09	–1	–1	–1	+1	174.53	1.72	77.57
R10	+1	–1	–1	+1	173.87	1.51	77.28
R11	–1	+1	–1	+1	157.32	2.07	69.92
R12	+1	+1	–1	+1	157.59	1.65	70.04
R13	–1	–1	+1	+1	174.18	1.57	77.41
R14	+1	–1	+1	+1	167.35	1.12	74.38
R15	–1	+1	+1	+1	152.64	1.69	67.84
R16	+1	+1	+1	+1	171.06	1.41	76.03
R17	–2	0	0	0	142.33	3.18	70.46
R18	+2	0	0	0	156.27	2.35	77.36
R19	0	–2	0	0	143.88	2.43	71.23
R20	0	+2	0	0	130.08	3.02	64.40
R21	0	0	–2	0	131.52	3.10	65.11
R22	0	0	+2	0	159.05	2.59	78.74
R23	0	0	0	–2	152.94	5.40	93.26
R24	0	0	0	+2	225.14	0.77	93.42
R25	0	0	0	0	178.26	2.77	88.25
R26	0	0	0	0	180.45	2.92	89.33
R27	0	0	0	0	180.86	2.74	89.53
R28	0	0	0	0	181.12	2.78	89.66
R29	0	0	0	0	180.47	2.86	89.34
R30	0	0	0	0	179.98	2.82	89.10
R31	0	0	0	0	179.24	2.76	88.73

(0) constituting the star points. The remaining 7 experimental runs comprised the variables at the intermediate (0) level constituting the 7 centre points.

2.5. Conducting the experiments as per the design matrix

Square butt joint configuration of size 100 mm × 100 mm × 6 mm was prepared and single pass butt welding procedure was employed to make the joints. Thirty-one weld runs were conducted randomly from the design matrix to prevent the effects of unknown nuisance variables contaminating the results [35]. A semi automatic FSW machine (manufactured by M/s RV Machine Tools, Coimbatore, India) shown in Fig. 3 was employed for this study. To carry out FSW as per the test runs detailed in the design matrix provided in Table 3, the tool rotational speed and welding speed were set as per the test run and the tool pin was allowed to plunge into the abutting surface of plates to be welded until the bottom of the tool shoulder touched the plates. Corresponding axial force as per the test run was set in the FSW machine and was acting on the plates through the shoulder for the various test runs. After a small dwell period the FSW machine table was moved at a required constant speed as per the design matrix. The axial force was

maintained till the end of that particular run. Dwell period is required to generate a frictional heat to bring the material to plastic state. Similarly all the remaining welding runs were carried out as given in the design matrix.

2.6. Recording the response parameters

Three tensile specimens were prepared from each of all thirty-one welded plates by cutting the welded plates perpendicular to the welding direction to the required dimensions as per ASTM: E8/E8 M-13a standard shown in Fig. 4a. The tensile test specimens fabricated from friction stir welded plates are shown in Fig. 4b. UTS and PE of the specimens were determined at room temperature using a Computerized Universal Testing Machine (HITECH TUE-C-1000). Average UTS and PE of friction stir welded composite joints and base composite are presented in Tables 3 and 4 respectively. Joint efficiency of welded composite [36] was calculated using Eq. (2) and the joint efficiency of all thirty-one welded joints is given in Table 3.

$$\text{Joint Efficiency, \%} = (\text{UTS}_{\text{welded joint}} / \text{UTS}_{\text{composite}}) \times 100 \quad (2)$$



Fig. 3. Photograph of friction stir welding machine.

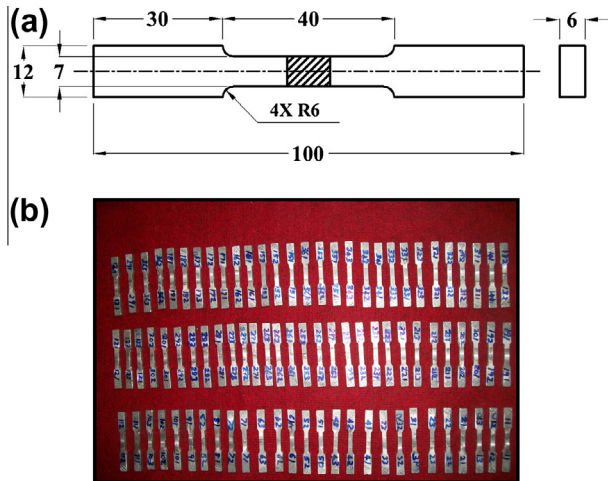


Fig. 4. Tensile test specimen: (a) dimensions per ASTM: E8/E8 M-13a standard and (b) prepared tensile specimens.

Table 4
UTS and PE of AA6061/AlN_p cast composite.

AlN _p (wt%)	0	5	10	15	20
UTS (MPa)	164	181	202	225	241
PE (%)	8.91	8.07	7.40	5.93	4.07

3. Development of regression models

The response functions UTS and PE of the friction stir welded joints are a function of tool rotational speed (N), welding speed (S), axial force (F) and percentage of AlN_p reinforcement (R). It can be expressed as given below [18,37,38]

$$\text{UTS or PE} = f(N, S, F, R) \quad (3)$$

The second order polynomial regression equation used to represent the response surface 'Y' is given by [34,35]

$$Y = b_0 + \sum b_i X_i + \sum b_{ii} X_i^2 + \sum b_{ij} X_i X_j \quad (4)$$

where b_0 is the average of responses and b_i and b_{ii} and b_{ij} are the response coefficients which depend on respective main and interaction effects of the parameters. The selected second order polynomial for four factors could be expressed as given below [34,35]

$$\begin{aligned} \text{UTS or PE} = & b_0 + b_1 N + b_2 S + b_3 F + b_4 R + b_{11} N^2 + b_{22} S^2 \\ & + b_{33} F^2 + b_{44} R^2 + b_{12} NS + b_{13} NF + b_{14} NR \\ & + b_{23} SF + b_{24} SR + b_{34} FR \end{aligned} \quad (5)$$

The coefficients were calculated using the software SYSTAT 12. All the coefficients were tested for their significance at 95% confidence level. The insignificant coefficients on response were removed without affecting the accuracy of the regression model to avoid the cumbersome mathematical labour [35]. The developed final regression model to predict UTS [39] and PE of friction stir welded joints with significant control parameters in coded form is given below.

$$\begin{aligned} \text{UTS, MPa} = & 182.386 + 2.644N - 4.853S + 1.553F + 13.148R \\ & - 7.895N^2 - 10.975S^2 - 8.899F^2 \end{aligned} \quad (6)$$

$$\text{PE, \%} = 2.814 - 0.191N + 0.146S - 0.16F - 1.268R + 0.079R^2 \quad (7)$$

4. Checking the adequacy of the developed models

The statistical results of the developed regression models are presented in Table 5. The predicted values of the responses will ideally match with the corresponding experimental results when the value of R^2 is one. As the obtained R^2 value for UTS and PE are 0.91 and 0.99 respectively the developed models are quite adequate. The adequacy of the developed regression models were also tested by analysis of variance (ANOVA) and the results are presented in Table 6. From Table 6 it was found that the calculated F -ratios are greater than the corresponding tabulated F -ratios at 95% confidence level. Hence, the developed models are quite adequate [35]. The regression models developed to predict the UTS and PE were further validated by plotting scatter diagram as shown in Figs. 5 and 6 respectively. The experimental values and the predicted values obtained from the regression models are scattered at both sides and are close to 45° line which clearly indicates good fitness of the developed regression models.

5. Validation of the regression models

To check the accuracy of the developed regression models, five weld runs were made on the AA6061/AlN_p composite using different values of tool rotational speed, welding speed and axial force other than those used in the design matrix. As mentioned earlier three tensile specimens were cut from each welded plate and its average UTS and PE were recorded. The percentage of error between the predicted and experimental UTS and PE were calculated and presented in Table 7. From the table it is evident that the accuracy of the model developed to predict the UTS is more than 93.73% and the model developed to predict the PE is more than 95.57%.

Table 5
Statistical results of the developed regression models.

Response	R^2	Adjusted R^2	Standard error
UTS	0.905	0.876	7.206
PE	0.990	0.988	0.126

Table 6
ANOVA results of the developed regression models.

Response	Source	Sum of squares	Degree of freedom	Mean-square	F ratio (calculated)	F ratio (tabulated)
UTS	Regression	11333.09	7	1619.01	31.18	2.44
	Residual	1194.31	23	51.93		
PE	Regression	40.77	5	8.15	516.33	2.60
	Residual	0.40	25	0.02		

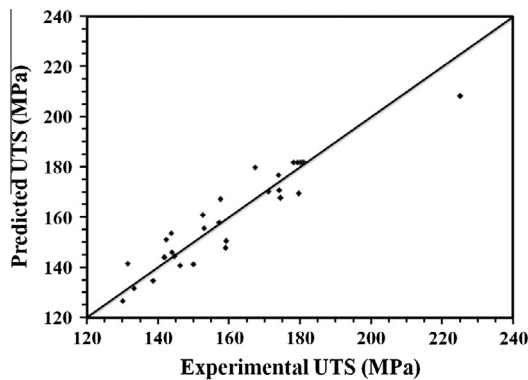


Fig. 5. Scatter diagram for UTS of friction stir welded AA6061/AlN_p composite.

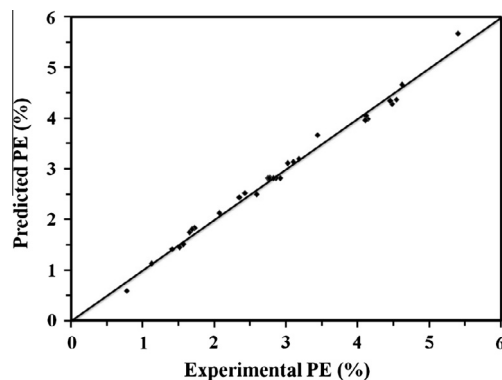


Fig. 6. Scatter diagram for PE of friction stir welded AA6061/AlN_p composite.

6. Results and discussions

AA6061/AlN_p composite was successfully friction stir welded as per the design matrix and the regression models for predicting UTS and PE were developed and presented in Eqs. (6) and (7) respectively. Both the developed regression models correlate the significant parameters *N*, *S*, *F* and *R* with their response functions such as UTS and PE of friction stir welded AA6061/AlN_p composite joints. It is obvious from the developed Eqs. (6) and (7) that there is no interaction effect of those parameters on the UTS and PE of friction

stir welded composite joints, as there is no significant coefficient for the interaction terms as *NS*, *NF*, *NR*, *SF*, *SR* and *FR*. Hence, these parameters independently influence the UTS and PE of friction stir welded composite joints.

The effects of these parameters on UTS and PE of welded joints are evaluated by using their corresponding developed regression models and the trends obtained for the above parameters are presented graphically in Figs. 7–10. The trend obtained for each parameter is in good agreement with the trend obtained by other researchers for the same process parameters [18,37]. The process parameters influence the frictional heat at the abutting surfaces of the plates which affects the plastic flow and consolidation of material. An optimal heat must be generated at the weld zone to obtain a defect free weld joint. When the heat generation at the weld zone falls short of or exceeds the optimal value, macro level defects are obtained that lead to poor joint strength. Some of the defects obtained at different conditions are presented in Table 8. From Tables 3 and 4, it is found that both UTS and PE of friction stir welded composite joints are less than those of corresponding base composite over the entire range of parameters studied in this work. The effects of these parameters on UTS and PE of friction stir welded joints are discussed below.

6.1. Effect of tool rotational speed

Fig. 7 depicts the effect of tool rotational speed on tensile behavior of friction stir welded AA6061/AlN_p composite joint. UTS of the weld joint initially increases with the increase in tool rotational speed from 1000 rpm to 1200 rpm, and reaches its maximum value when tool rotational speed is 1200 rpm then it decreases with further increase in tool rotational speed. The PE of the welded joints decreases with the increase in tool rotational speed.

Tool rotational speed is responsible for stirring and mixing of plasticized material around the rotating tool pin which in turn increase the temperature of the plasticized material. When the tool rotational speed increases (above 1200 rpm) higher heat is generated in the stir zone due to increase of relative velocity between rotating tool and the substrate. Increased heat input increases grain growth and dissolution of Mg₂Si precipitates at weld zone [37]. In addition, higher heat input does not promote the nucleation of grains and precipitation of Mg₂Si [25]. When tool rotational speed is increased beyond 1200 rpm heat generated at the weld zone increases resulting in turbulence of strained plasticized

Table 7
Results of conformity tests for the developed regression models.

Test run	Process parameters				Experimental value		Predicted value		% of Error	
	<i>N</i>	<i>S</i>	<i>F</i>	<i>R</i>	UTS (MPa)	PE (%)	UTS (MPa)	PE (%)	UTS	PE
1	1.5	0.5	−1.25	−2	127.63	5.40	121.28	5.65	5.24	−4.43
2	0.50	1.25	−0.25	−1	138.45	4.11	144.43	4.29	−4.14	−4.05
3	−0.25	−0.50	0.75	0	171.40	2.76	177.07	2.67	−3.21	3.48
4	−1.25	1.75	1.25	1	133.71	1.86	125.83	1.92	6.27	−3.26
5	−1.75	−0.75	1.75	2	157.58	0.56	152.81	0.54	3.12	3.38

% of Error = [(experimental value – predicted value)/predicted value] × 100.

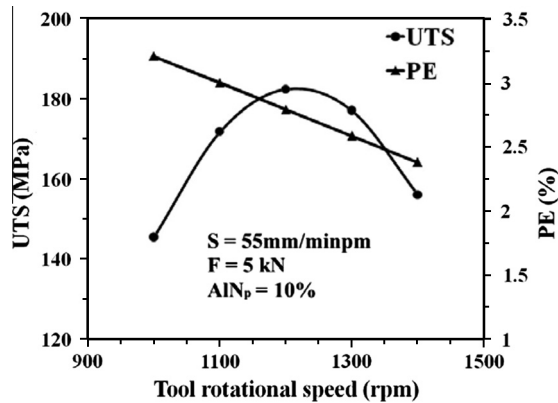


Fig. 7. Effect of tool rotational speed on UTS and PE of friction stir welded AA6061/AlN_p composite.

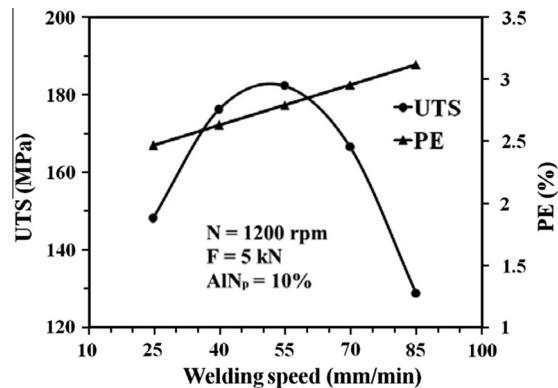


Fig. 8. Effect of welding speed on UTS and PE of friction stir welded AA6061/AlN_p composite.

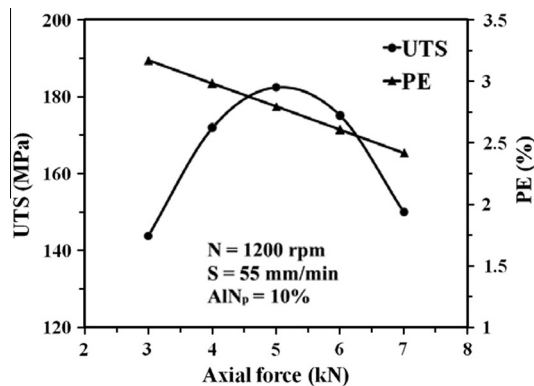


Fig. 9. Effect of axial force on UTS and PE of friction stir welded AA6061/AlN_p composite.

materials and formation of macro level defects at the weld zone. All these effects lead to poor joint with inferior tensile strength. At lower tool rotational speed below 1200 rpm, heat generation at the weld zone is inadequate to strain the plasticized material resulting in poor consolidation of material and formation of tunnel defect at the retreating side. This results in the joint having lower tensile strength. Hence optimum tool rotational speed is essential to generate adequate frictional heat, as it produces sufficient straining of plasticized material with fine recrystallized grains

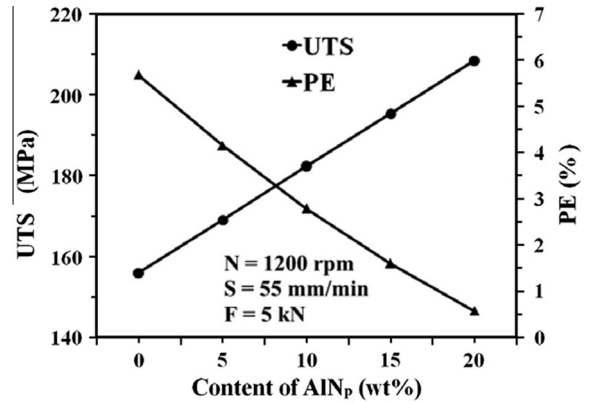


Fig. 10. Effect of percentage of AlN_p reinforcement in the AA6061 matrix on UTS and PE of friction stir welded AA6061/AlN_p composite.

resulting in defect free joints [18]. Higher tool rotational speed influences straining rate of plasticized material, change in grain size, precipitation of Mg₂Si and inclusion of wear debris of tool in the weld zone. All these effects decreased the PE of the welded joint.

6.2. Effect of welding speed


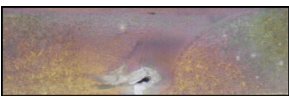
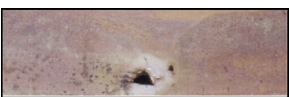


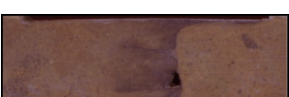
The effect of welding speed on tensile behavior of friction stir welded AA6061/AlN_p composite joint is presented in Fig. 8. As the welding speed increases from 25 mm/min to 55 mm/min, UTS of weld joint increases and reaches its maximum value when welding speed is 55 mm/min, then it decreases with subsequent increase in the welding speed. The elongation of the welded joints increases with increase in welding speeds.

The translation of the rotating tool transports the stirred plasticized material from the front to back of the tool pin. During the FSW thermal cycle, rate of heat at the weld zone is a strong function of welding speed. Welding speed has inverse effect on the heat generation at the weld zone and determines the exposure time of the frictional heat per unit length of the weld and as a result influences the grain growth. The joint made with the welding speed of 55 mm/min have higher tensile strength with defect free weld joint which may be attributed to transportation of sufficient plasticized material and good consolidation of material with fine grains. At lower welding speed (below 55 mm/min) higher heat is generated due to the longer exposure time to frictional heat per unit length of the weld area and rate of cooling is decreased which leads to coarsening of grains and affects the Mg₂Si precipitates [25].

The excess turbulence of flowing metal is also possible due to high heat generation which changes the regular flow pattern of plasticized material resulting in formation of macro level defect in the weld zone. Due to the shorter exposure time to the frictional heat per unit length of the weld area at higher welding speed above 55 mm/min, less heat is generated which results in faster cooling rate of the welded joint. This can appreciably reduce the degree of metallurgical transformations taking place during welding (such as solubilization, re-precipitation and coarsening of precipitates) resulting in reduction of strength of individual regions across the weld zone [37]. Lesser heat input at weld zone at higher welding speed causes insufficient plasticized material transportation from advancing side to the retreating side and reduction in the softened area due to faster cooling rates [21] which lead to macro level defects like tunnels in weld region. Lower welding speed influences straining rate of plasticized material, change in grain size, precipitation of Mg₂Si and inclusion of wear debris of

Table 8

Typical macro defects obtained when heat generation at the weld zone is fall short of or exceed the optimized value.

S.No.	Process parameters	Macrostructure	Remark	Probable reason
1	$N = 1000$ rpm $S = 55$ mm/min $F = 5$ kN		Tunnel defect	Insufficient heat generation
2	$N = 1400$ rpm $S = 55$ mm/min $F = 5$ kN		Worm hole	Excessive stirring & flow of plasticized material – High frictional heat generation
3	$S = 25$ mm/min $N = 1200$ rpm $F = 5$ kN		Piping defect	Insufficient consolidation of material due to excess turbulence – High frictional heat generation
4	$S = 85$ mm/min $N = 1200$ rpm $F = 5$ kN		Tunnel defect	Insufficient heat generation
5	$F = 3$ kN $S = 55$ mm/min $N = 1200$ rpm		Tunnel defect	Less heat generation and poor consolidation
6	$F = 7$ kN $S = 55$ mm/min $N = 1200$ rpm		Worm hole & thinning at weld zone	More plunge depth - High frictional heat generation

tool in the weld zone. All those effects contribute to the increasing trend of PE.

6.3. Effect of axial force

Fig. 9 reveals the effect of axial force on tensile behavior of friction stir welded AA6061/AlN_p composite joint. UTS of friction stir welded composite joint initially increases with the increase of the axial force from 3 kN to 5 kN, and reaches its maximum value when the axial force is 5 kN. UTS decreases with further increase in the axial force from 5 kN to 7 kN. The elongation of the welded joint decreases with the increase in axial force.

Axial force is responsible to form inter-atomic forces to make a solid state welding. Bonding occurs when a pair of surfaces is brought together in the vicinity of inter-atomic-forces [28]. The frictional force between the rotating tool and the substrate is dependent upon the axial force and the coefficient of friction. As the coefficient of friction depends on the surface roughness of contacting surfaces, frictional forces varies with varying axial load. Hence higher axial force increases the frictional force which in turn increases the amount of heat generated beneath the shoulder [18].

Flow stress of the material decreases when the temperature beneath the shoulder increases and vice-versa. Hence optimum temperature and axial force are necessary to obtain sound joints. When the axial force is 5 kN, the hydrostatic pressure beneath the shoulder may just exceed the flow stress of the material at the generated temperature facilitating sufficient extrusion of the plasticized

material and proper consolidation of the material. All those positive effects lead to defect free sound weld joint with higher tensile strength. At lower axial forces (below 5 kN), hydrostatic pressure under the shoulder may be less which leads to less heat generation, insufficient material transportation and poor consolidation resulting in formation of tunnel defect leading to inferior joint strength. At higher axial force (above 5 kN), heat generation at weld zone increases which reduces the flow stress. As a result, plasticized material come out on both advancing and retreating sides as shear lips. Hence, higher axial force leads to thinning of weld joint which results in lower tensile strength of welded joint. The axial force influences the straining rate of plasticized material, change in grain size and Mg₂Si precipitation in the weld zone. All these effects contribute to the decreasing trend of PE.

6.4. Effect of reinforcement

Fig. 10 depicts the effect of weight percentage of AlN_p reinforcement on tensile behavior of friction stir welded AA6061/AlN_p composite joint. It is obvious that UTS of the AMC increases with the increase in the amount of AlN_p reinforcement in the matrix. But the elongation of the welded joints decreases with the increase in content of AlN_p reinforcement.

In AMCs, an increase in the volume fraction of the hard ceramic reinforcing particulates increases dislocation density and reduces grain size and the amount of substructure. These microstructural changes tend to increase the resistance offered to the motion of

mobile dislocations under the influence of a far-field stress. Hence, an increase in the weight percentage of AlN_p reinforcement in the aluminium alloy matrix increases the magnitude of resistance offered to the motion of dislocations resulting in increased UTS [40].

Application of FSW closes the presence of porosity in cast materials [23]. Stirring action of the tool shattered the agglomerated particles present in the base composite into homogeneous distribution. Due to the abrasive action of the hard rotating square profile pin tool the ceramic reinforcement particles are broken into smaller size and distributed uniformly [19,33]. Uniform distribution of AlN_p reinforcement also increases the UTS as it increases the load bearing capacity of the composite [41]. Hence, UTS of the friction stir welded composite increases with increasing percentage of reinforcement. Increasing the weight percentage of AlN_p in the composite resists the flowability of aluminium alloy matrix, reduces the ductile aluminium alloy matrix content which results in the decrease of PE of the composite. Intense stirring and severe plasticization of material lead to grain refinement and reduction of grain size in the friction stir welded zone. Grain boundary is one of the major hurdles to the movement of dislocations. As there is large grain boundary per unit volume in the weld zone, PE of the friction stir welded composite joint is less than the corresponding base composite.

7. Optimization

The FSW parameters significantly influence the UTS and PE of the welded joints. It is necessary to choose exact combination of parameters such that the joint will have maximum UTS and maximum PE. To have higher productivity higher UTS and PE have to be achieved at higher welding speed. The developed regression models were used to optimize the FSW parameters. The optimization is a nonlinear constrained maximization problem and is solved using generalized reduced gradient (GRG) method. The GRG is embedded in the optimization tool available in a software package and the algorithm is given below. A complete GRG application for process optimization is available elsewhere [42].

Step 1. Choose:

- a starting set of variable V^0 of feasible V_i^0 s
- an initial number of iterations N_s
- an accuracy ε for convergence and stopping

Set $p = 1$ (iteration counter)

Step 2. Identify basic, non/basic and super/basic variables

If $p = 1$, variables that are not basic are set to be super/basic
Calculate search direction G_R
Calculate an optimum step size
Calculate V^p

Step 3. Convergence and Termination

Convergence for GRG

If the Kuhn–Tucker conditions are satisfied then STOP.

Stopping Criteria

- Variable increment $\Delta V = |V^p - V^{p/1}|$
If $\Delta V < \varepsilon$ then STOP.
- If $p = N_s$
Find the extrapolated maximum number of iterations N_{max}
If $N_{max} > N_s$ then set $N_s = N_{max}$ else STOP.
Continue to the next iteration (increment p by one)
Go to step 2

The developed regression models were optimized in four different situations as follows:

1. Optimization of FSW parameters for maximum UTS (OP1)

The objective function selected for optimization was to maximize the UTS as given in Eq. (6) subject to the following constraints:

$$-2 \leq N \leq +2, -2 \leq S \leq +2, -2 \leq F \leq +2 \& -2 \leq R \leq +2$$

2. Optimization of FSW parameters for maximum UTS at higher welding speed (OP2)

The objective function selected for optimization was to maximize the UTS as given in Eq. (6) for possible maximum welding speed subject to the following constraints:

$$-2 \leq N \leq +2, 0.25 \leq S \leq +2, -2 \leq F \leq +2 \& -2 \leq R \leq +2$$

3. Optimization of FSW parameters for maximum UTS and PE (OP3)

The objective function selected for optimization was to maximize the UTS and PE simultaneously as given in Eqs. (6) and (7) subject to the following constraints:

$$-2 \leq N \leq +2, -2 \leq S \leq +2, -2 \leq F \leq +2, -1 \leq R \leq +2, 180 \leq UTS \& 2 \leq PE$$

4. Optimization of FSW parameters for maximum UTS and PE at higher welding speed (OP4)

The objective function selected for optimization was to maximize the UTS and PE simultaneously as given in Eqs. (6) and (7) for possible higher welding speed subject to the following constraints:

$$-2 \leq N \leq +2, 0.25 \leq S \leq +2, -2 \leq F \leq +2, -1 \leq R \leq +2, 190 \leq UTS \& 1 \leq PE$$

The optimized FSW parameters for those four situations along with predicted values of the responses are given in Table 9. The welded matrix alloy was not considered in the optimization involving PE (OP3 & OP4).

Conformity tests were conducted to validate the optimization. FSW was carried out using the optimized process parameters OP1, OP2 and OP4 provided in Table 9. Three tensile specimens were prepared from each welded plate to record the UTS and PE. The average UTS and PE are presented in Table 10. The maximum percentage of error obtained in UTS between the predicted and experimental value was 8.36. The macrostructure of the welded

Table 9
Optimized FSW parameters and predicted UTS and PE.

Optimized condition	Parameters				Optimized values	
	N (rpm) Coded/actual	S (mm/min)	F (kN)	R (wt%)	UTS (MPa)	PE (%)
OP1	0.17/1217	−0.22/51.68	0.09/5.09	2/20	209.51	0.52
OP2	0.17/1217	0.25/58.75	0.087/5.09	2/20	207.07	0.59
OP3	0.031/1203	−0.15/52.81	−0.01/4.99	0/10	182.91	2.79
OP4	0.03/1203	0.25/58.75	−0.02/4.98	1.0/15	193.68	1.66

Table 10

Results of conformity tests for optimization.

Optimized condition	Optimized values		Experimental values		% of Error	Joint efficiency (%)
	UTS (MPa)	PE (%)	UTS (MPa)	PE (%)		
OP1	209.51	0.52	227.02	0.70	−8.36	94.28
OP2	207.07	0.59	217.36	0.86	−4.97	90.19
OP4	193.68	1.66	202.46	1.42	−4.53	89.98

Table 11

Macrostructure of friction stir welded joint made by OP1 process parameters values.

S.No.	Process parameters	Macrostructure	Remark	Probable reason
1	$F = 5.08 \text{ kN}$ $S = 51.81 \text{ mm/min}$ $N = 1217 \text{ rpm}$		No defect	Optimum frictional heat generation and good consolidation

joint fabricated by the optimized FSW parameters (OP1) presented in Table 11 exhibited the defect free weld joint.

8. Conclusions

The following conclusions are derived from the above investigations.

- The regression models were developed to predict the UTS and PE of friction stir welded AA6061/AlN_p composite joints.
- Conformity tests were conducted to validate the developed regression models. The models were found to be accurate.
- The parameters considered in this study such as tool rotational speed, welding speed, axial force and percentage of reinforcement independently influenced the UTS and PE of the friction stir welded joints over the entire range of parameters studied in this work.
- FSW process parameters were optimized to maximize the UTS under various situations by using the generalized reduced gradient method.
- Conformity tests were conducted to validate the optimization. UTS of the joint fabricated using the optimized FSW parameters (OP1) is found to be maximum.
- UTS and PE of AA6061/20 wt% AlN_p composite joint made with OP1 condition is about 1% greater and 9.1% lesser than that of AA6061/20 wt% AlN_p composite joint made as per the design matrix.
- Joint efficiency of the friction stir welded AA6061/20 wt% AlN_p composite with OP1 condition is 94.28% which is 1% greater than that of the AA6061/20 wt% AlN_p composite made as per the design matrix.

Acknowledgements

The authors wish to place their sincere thanks to Naval Research Board, DRDO, Govt. of India for providing funds to purchase friction Stir Welding Machine (vide funded project: Ref. No. DNRD/05/4003/NRB/85 Dated 30.10.2006). Authors are grateful to the department of Mechanical Engineering, Coimbatore Institute of Technology, Coimbatore, India for extending the facilities of Welding Research Laboratory to carry out this research work. The authors are grateful to Karunya University, Coimbatore, India for providing UTM testing facility. Authors are also thankful to Mr. S.J. Vijay, Dr. I. Dinaharan, Mr. R. Sathiskumar, Mr. R.D. Vasudevan,

Mrs. S. Hemamalini, Mr. K. Raja and Dr. V. Rajasekaran for their assistance to execute this work.

References

- [1] Hooker JA, Doorbar PJ. Metal matrix composites for aeroengines. *Mater Sci Technol* 2000;16:72531.
- [2] Liu YB, Lim SC, Lu L. Recent development in the fabrication of metal matrix particulate composites using powder metallurgy technology. *J Mater Sci* 1994;29:19992007.
- [3] Kaw AK. *Mechanics of composite materials*. 2nd ed. London (New York): Taylor & Francis Group; 2006.
- [4] Storjohann D, Barabash OM, Babu SS, David SA, Sklad PS, Bloom EE. Fusion and friction stir welding of aluminium–metal–matrix composites. *Metall Mater Trans A* 2005;36A:3237–47.
- [5] Thomas WM, Nicholas ED, Needham JC, Murch MG, Temple-Smith P, Dawes CJ. Friction-stir butt welding, GB Patent No. 9125978.8, International patent application No. PCT/GB92/02203, 1991.
- [6] Cavaliere P, Campanile G, Panella F, Squillace A. Effect of welding parameters on mechanical and microstructural properties of AA6056 joints produced by friction stir welding. *J Mater Process Technol* 2006;180(1–3):263–70.
- [7] Nandan R, Roy GG, Lienert TJ, Debroy T. Three-dimensional heat and material flow during friction stir welding of mild steel. *Acta Materialia* 2007;55:883–95.
- [8] Esparza JA, Davis WC, Trillo EA, Murr LE. Friction-stir welding of magnesium alloy AZ31B. *J Mater Sci Lett* 2002;21(12):917–20.
- [9] Lee Won-Bae, Jung Seung-Boo. The joint properties of copper by friction stir welding. *Mater Lett* 2004;58(6):1041–6.
- [10] Fjii FYH, Tsumura T, Nakata K. Friction stir welding of Inconel alloy 600. *J Mater Sci* 2006;41:5376–9.
- [11] Sato YS, Nelson TW, Sterling CJ, Steel RJ, Pettersson C-O. Microstructure and mechanical properties of friction stir welded SAF 2507 super duplex stainless steel. *Mater Sci Eng A* 2005;397(1–2):376–84.
- [12] Cui L, Fujii H, Tsuji N, Nogi K. Friction stir welding of a high carbon steel. *Scr Mater* 2007;56(7):637–40.
- [13] Uzun Huseyin. Friction stir welding of SiC particulate reinforced AA2124 aluminium alloy matrix composite. *Mater Des* 2007;28(5):1440–6.
- [14] Ceschini L, Boromei I, Minak G, Morri A, Tarterini F. Effect of friction stir welding on microstructure, tensile and fatigue properties of the AA7005/10 vol.%Al₂O_{3p} composite. *Compos Sci Technol* 2007;67(3–4):605–15.
- [15] Chen XG, Silva MD, Gougeon P, St-Georges L. Microstructure and mechanical properties of friction stir welded AA6063–B₄C metal matrix composites. *Mater Sci Eng A* 2009;518(1–2):174–84.
- [16] Christy TV, Murugan N. Prediction of tensile strength of friction stir welded Al–TiB₂ composite plates using a mathematical model. *Int J Emerg Technol Appl Eng Technol Sci* 2010;3(1):566–72.
- [17] Gopalakrishnan S, Murugan N. Prediction of tensile strength of friction stir welded aluminium matrix TiC_p particulate reinforced composite. *Mater Des* 2011;32(1):462–7.
- [18] Dinaharan I, Murugan N, Parameswaran S. Developing an empirical relationship to predict the influence of process parameters on tensile strength of friction stir welded AA6061/0–10 wt% ZrB₂ in situ composite. *Trans Indian Inst Met* 2012;65(2):159–70.

- [19] Marzoli LM, Strombeck AV, Santos JFD, Gambaro C, Volpone LM. Friction stir welding of an AA6061/Al₂O₃/20_p reinforced alloy. *Compos Sci Technol* 2006;66:363–71.
- [20] Cam G. Friction stir welded structural materials: beyond Al-alloys. *Int Mater Rev* 2011;56(1):1–48.
- [21] Karthikeyan L, Senthilkumar VS, Padmanabhan KA. On the role of process variables in the friction stir processing of cast aluminium A319 alloy. *Mater Des* 2010;31:761–71.
- [22] Jayaraman M, Sivasubramanian R, Balasubramanian V, Lakshminarayanan AK. Effect of process parameters on tensile strength of friction stir welded cast LM6 aluminium alloy joints. *J Mater Sci Technol* 2009;25:655–64.
- [23] Azimzadegan T, Serajzadeh S. An investigation into microstructures and mechanical properties of AA7075–T6 during friction stir welding at relatively high rotational speeds. *J Mater Eng Perform* 2010;19:1256–63.
- [24] Sakthivel T, Sengar GS, Mukhopadhyay J. Effect of welding speed on microstructure and mechanical properties of friction stir welded aluminium. *Int J Adv Manuf Technol* 2009;43:468–73.
- [25] Elangovan K, Balasubramanian V. Influences of tool pin profile and welding speed on the formation of friction stir processing zone in AA2219 aluminium alloy. *J Mater Process Technol* 2008;20:163–75.
- [26] Kumar K, Kailas SV. On the role of axial load and the effect of interface position on the tensile strength of a friction stir welded aluminium alloy. *Mater Des* 2008;29(4):791–7.
- [27] Elangovan K, Balasubramanian V, Valliappan M. Influences of tool pin profile and axial force on the formation of friction stir processing zone in AA6061 aluminium alloy. *Int J Adv Manuf Technol* 2008;38:285–95.
- [28] Seighalani KR, Givi MKB, Nasiri AM, Bahemmat P. Investigations on the effects of the tool material, geometry, and tilt angle on friction stir welding of pure titanium. *J Mater Eng Perform* 2010;19:955–62.
- [29] Vijay SJ, Murugan N. Influence of tool pin profile on the metallurgical and mechanical properties of friction stir welded Al–10 wt% TiB₂ metal matrix composite. *Mater Des* 2010;31(7):3585–9.
- [30] Fogagnolo JB, Robert MH, Torralba JM. Mechanically alloyed AlN particle-reinforced Al-6061 matrix composites: powder processing, consolidation and mechanical strength and hardness of the as-extruded materials. *Mater Sci Eng A* 2006;426:85–94.
- [31] Liu YQ, Cong HT, Wang W, Sun CH, Cheng HM. AlN nanoparticle-reinforced nanocrystalline Al matrix composites: fabrication and mechanical properties. *Mater Sci Eng A* 2009;505:151–6.
- [32] Ashok Kumar B, Murugan N. Metallurgical and mechanical characterization of stir cast AA6061–T6–AlN_p composite. *Mater Des* 2012;40:52–8.
- [33] Feng AH, Xiao BL, Ma ZY. Effect of microstructural evolution on mechanical properties of friction stir welded AA2009/SiCp composite. *Compos Sci Technol* 2008;68:2141–8.
- [34] Murugan N, Parmar RS. Effects of MIG process parameters on the geometry of the bead in the automatic surfacing of stainless steel. *J Mater Process Technol* 1994;41:381–98.
- [35] Montgomery DG. Design and analysis of experiments. 5th ed. New York: John Wiley & sons; 2001.
- [36] Lakshminarayanan AK, Balasubramanian V, Elangovan K. Effect of welding processes on tensile properties of AA6061 aluminium alloy joints. *Int J Adv Manuf Technol* 2009;40:286–96.
- [37] Elangovan K, Balasubramanian V, Babu S. Predicting tensile strength of friction stir welded AA6061 aluminium alloy joints by a mathematical model. *Mater Des* 2009;30(1):188–93.
- [38] Sundaram NS, Murugan N. Tensile behavior of dissimilar friction stir welded joints of aluminium alloys. *Mater Des* 2010;31(9):4184–93.
- [39] Murugan N, Ashok Kumar B. Prediction of tensile strength of friction stir welded stir cast AA6061–T6/AlNp composite. *Mater Des* 2013;51:998–1007.
- [40] Gupta M, Srivatsan TS. Interrelationship between matrix microhardness and ultimate tensile strength of discontinuous particulate-reinforced aluminium alloy composites. *Mater Lett* 2001;51(3):255–61.
- [41] Tjong SC, Ma ZY. Microstructural and mechanical characteristics of in situ metal matrix composites. *Mater Sci Eng R* 2000;29(3–4):49–113.
- [42] Soontrapa C, Chen Y. Optimization approach in variable-charge potential for metal/metal oxide systems. *Comput Mater Sci* 2009;46:887–92.